NOAA Technical Memorandum NMFS
This TM series is used for documentation and timely communication of preliminary results, interim reports, or special purpose information. The TMs have not received complete formal review, editorial control, or detailed editing.

1996

COASTAL UPWELLING INDICES WEST COAST OF NORTH AMERICA 1946-95

Franklin B. Schwing

Michael O'Farrell

John M. Steger

Kenneth Baltz

Pacific Fisheries Environmental Laboratory
Southwest Fisheries Science Center
1352 Lighthouse Avenue
Pacific Grove, California 93950-2097

NOAA-TM-NMFS-SWFSC-231

U.S. DEPARTMENT OF COMMERCE

National Oceanic and Atmospheric Administration

National Marine Fisheries Service

Abstract

Long time series of ocean surface currents are not available, however reasonable estimates of surface transport and coastal upwelling may be made using planetary boundary layer theory and the geostrophic wind approximation. PFEG generates daily and monthly indices of coastal upwelling at 15 standard geographic points along the west coast of North America. The first set, beginning in 1967, is comprised of daily means of six-hourly upwelling indices, estimated from six-hourly synoptic pressure fields. The second set of indices are derived from monthly-mean pressure fields, and extend back over 50 years to 1946.

The annual cycle is estimated at each point by a least-squares regression of the 1967-91 daily data to an annual and semiannual harmonic signal. The means and standard deviations of monthly values are calculated for the same 25-year period to compare their annual climatologies to those from the daily indices. Upwelling north of 30^oN has a strong annual signal. Greatest upwelling rates occur at 33^oN, with a linear decrease in the maximum upwelling indices north to about 54^oN. The greatest annual range occurs at 39^oN. The date of maximum upwelling increases linearly from late April at 21^oN to mid-July at 48^oN. Minima occur within 15 days of 1 January at all latitudes, with negative (downwelling-favorable) indices occurring north of 36^oN during at least part of the year. Downwelling is a year-around feature along the British Columbia coast. The annual range off Baja California is relatively small. This region is also characterized by secondary minima and maxima in August and October, respectively. Highest interannual variance at a location occurs during months of greatest absolute index values. Variance south (north) of 45^oN is greatest in summer (winter).

Indices derived from monthly pressure fields are consistently greater than monthly averages of the daily indices. This discrepancy is greatest during winter downwelling at northern points, and summer upwelling at southern points. Daily standard errors are consistently greater than the associated monthly deviations, due to the high variability on a given Julian day associated with synoptic atmospheric motions. Monthly standard deviations off central and southern California peak in spring and remain relatively high through the summer, while daily standard errors decline rapidly between late winter and summer.

One of the most striking highlights is the relatively short duration of significant positive and negative anomalies ($<$ 1 year), despite the large latitudinal extent of most anomalies. The indices also feature sudden shifts in their temporal patterns. These may be attributed to changes in the source of the monthly pressure fields, or in the methodology used to interpolate the gridded pressure fields used to calculate these indices, rather than true environmental changes.

Introduction

The frictional stress of equatorward wind on the ocean's surface, in concert with the earth's rotation, causes water in the surface layer to move away from the western coast of continental land masses (Sverdrup *et al.* 1942, p. 501). The offshore moving surface water, referred to as Ekman transport after the scientist who first described this process, is replaced by water which upwells along the coast from depths of 50-100 m and more. Upwelled water is cooler and more saline than the original surface water (Robinson 1976; Huyer 1983; Kosro *et al.* 1991) and typically has much greater concentrations of nutrients such as nitrate, phosphate and silicate that are key to sustaining biological production (Smith 1968; Traganza *et al.* 1981; Kosro *et al.* 1991). This is why marine ecosystems in eastern boundary currents are highly productive, and capable of maintaining large standing crops of plankton, massive fish stocks such as sardines and anchovies, and major populations of marine mammals and sea birds (Cushing 1969; Ryther 1969; Walsh *et al.* 1977; Wroblewski 1977). The major eastern boundary currents include the Canary off the Iberian peninsula and northwestern Africa, the Benguela off southwestern Africa, the Peru (or Humboldt) off western South America, the Leeuwin off western Australia, and the California Current System off western North America. Moreover variations in upwelling over seasonal to interannual and longer periods, due to large-scale shifts in wind patterns and atmospheric systems, are linked to variability in fish populations and other biological components in coastal ocean ecosystems (Parrish *et al.* 1981; Cury *et al.* 1995; Parrish and Mallicoate 1995).

Each month, the Pacific Fisheries Environmental Group (PFEG) generates indices of the intensity of large-scale, wind-induced coastal upwelling at 15 standard locations along the west coast of North America (Figure 1). The indices are based on estimates of offshore Ekman transport driven by geostrophic wind stress. Geostrophic winds are derived from six-hourly synoptic and monthly mean surface atmospheric pressure fields. The pressure fields are interpolated from surface observations and provided by the U.S. Navy Fleet Numerical Meteorology and Oceanography Center (FNMOC), Monterey, CA.

Directly quantifying upwelling is extremely difficult, and observed time series of the phenomenon do not exist. The idea behind the upwelling index was to develop some simple time series that represent variations in upwelling along the coast. Wooster and Reid (1963) demonstrated that the offshore component of surface Ekman transport represents an "index of upwelling" that describes seasonal variability in near-coastal cooling presumably associated with upwelling. Although long-term time series of ocean surface currents are not available, reasonable estimates of surface transport may be made using the geostrophic wind approximation and planetary boundary layer theory. PFEG regularly produces and provides daily and monthly index time series to scientists

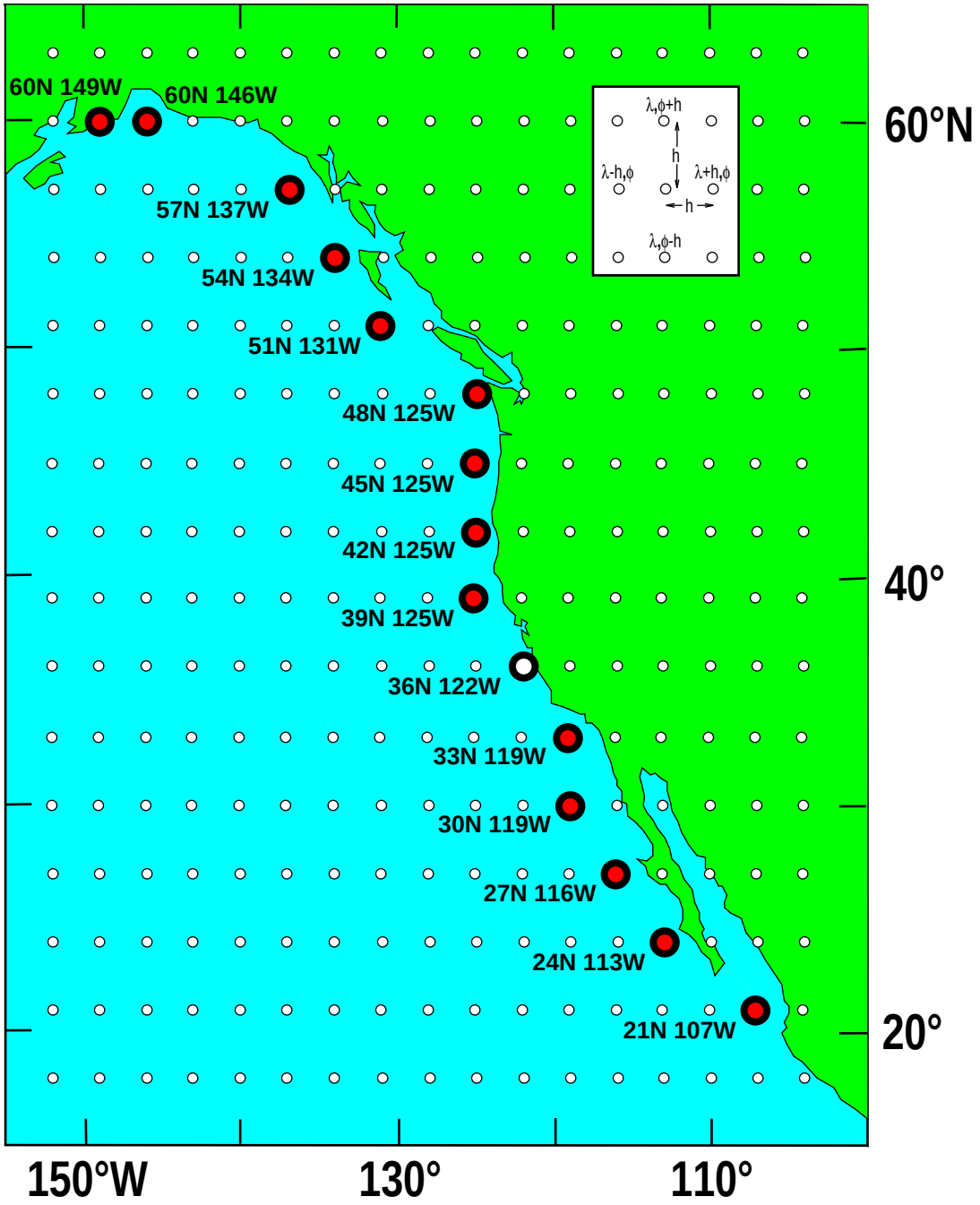

Figure 1. Map showing 3^{o} extrapolated mesh (small open circles) for pressure fields used to derive the upwelling indices. Large open circles denote locations of the 15 standard near-coastal positions of the indices reported here. Inset shows discretization scheme used to estimate geostrophic winds from pressure gradients (Equations 1 and 2).

and managers concerned with marine ecosystems and their biota. The indices are currently distributed to about 50 regular users each month, and each year another 40-50 individuals request upwelling data or information on how they are derived. The distribution of users by their afiliation is shown in Figure 2. The chart on the left represents the distribution of individuals receiving upwelling index data on a monthly basis, while the chart on the right denotes the afiliation of individuals who have requested data or information since 1984.

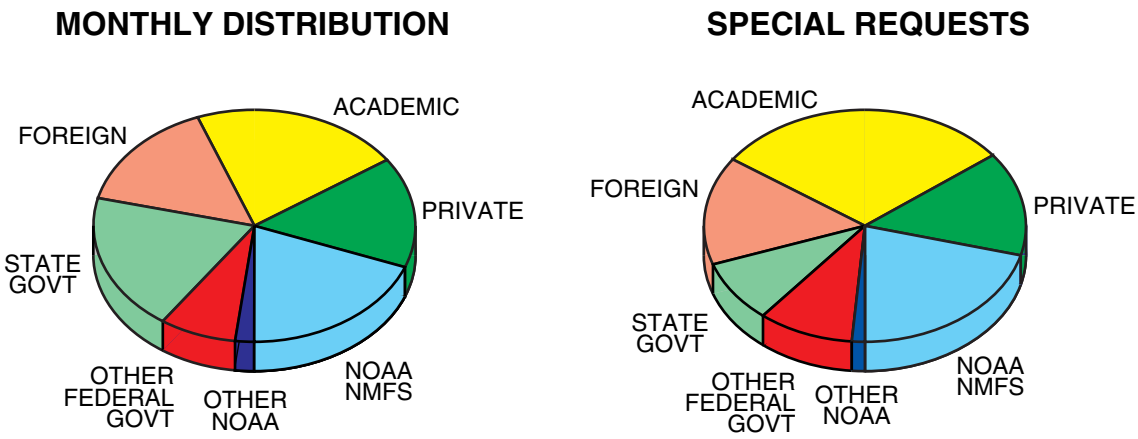

Figure 2. Charts showing the distribution of users of upwelling index data and related information,by their type of affiliation. Left hand chart shows distribution of individuals receiving upwelling products on a monthly basis. Right hand chart shows distribution of special requests for upwelling products or information.

These series have been used in scores of studies and scientific publications; over 400 publications refer to the Bakun (1973) technical memorandum that initially described the upwelling indices. Examples include studies to describe coastal circulation (Bakun and Nelson 1977; Huyer 1983; Hayward et al. 1995; Thomson and Ware 1996); ENSO (Huyer and Smith 1985); and climate change (Bakun 1990; van Geen and Husby 1996); as well as in understanding the linkages between environmental and biological variability; zooplankton (Peterson and Miller 1977; Brodeur and Ware 1992), crabs (Botsford and Wickham 1975; McConnaughey et al. 1992), groundfish (Ainley et al. 1993; VenTresca et al. 1995), small pelagics (Parrish and MacCall 1978; Cury and Roy 1989; Parrish and Mallicoate 1995), salmon (Nickelson 1986; Fisher and Pearcy 1988; Hiss 1995), and marine birds (Ainley et al. 1993, 1995).

PFEG coastal upwelling indices are calculated based upon Ekman's (1905) theory of mass transport due to wind stress. Assuming homogeneity, uniform wind, and steady state conditions, the mass transport of surface water due to wind stress is 90^o to the right of the wind direction in the Northern Hemisphere. Ekman mass transport is defined as the wind stress divided by the Coriolis parameter. The depth to which an appreciable amount of this offshore transport occurs is termed the surface Ekman layer, and is generally 50-100 m deep.

Ekman transports are resolved into components parallel and normal to the local coastline orientation. The magnitude of the offshore component is considered to be an index of the amount of water upwelled from the base of the Ekman layer. Positive values are, in general, the result of equatorward wind stress. Negative values imply downwelling, the onshore advection of surface waters accompanied by a downward displacement of water.

History of the Upwelling Index

PFEG began computing the upwelling indices in the early 1970's. Six-hourly synoptic surface pressure analyses from FNMOC, originally known as Fleet Numerical Weather Central and later as Fleet Numerical Oceanographic Center, were used to calculate two sets of upwelling index time series. One set is comprised of daily and weekly means of six-hourly upwelling indices, estimated from the FNMOC six-hourly synoptic pressure fields. Availability of synoptic data prior to 1967 is much more limited. The second set of indices are monthly time series derived from monthly-mean pressure fields, and extend back to 1946. The synoptic fields used to construct the monthly mean fields prior to July 1962 were acquired from a variety of sources (Bakun 1973), rather than FNMOC.

Bakun (1973) initially described the methods used to calculate the upwelling indices, and presented monthly, quarterly, and annual indices for 15 near-coastal positions along the North American west coast for the period 1946-71. Daily and weekly means of the upwelling indices at these standard west coast locations were published by Bakun (1975) for the period 1967-73. A third report in the series (Mason and Bakun 1986) summarizes the monthly indices for 1946-71, along with daily and weekly means of the six-hourly indices for 1974-85 at six locations along the U.S. west coast (33-48^{o}N). Because of differences in the averaging period of the pressure fields, the daily and monthly series are not numerically equivalent nor directly interchangeable (cf. average annual cycles derived from daily and monthly values).

Methods

Bakun (1973) describes the computations for deriving the upwelling indices. Due to limited availability of that publication, the assumptions and calculations will be detailed here as well.

Historically, six-hourly and monthly mean pressure fields prepared by FNMOC on a 63 × 63 point square grid were superimposed onto a polar-stereographic projection of the Northern Hemisphere. The mesh length of this projection is 200 nm (370 km) at 60^{o}N and decreases southward to about 144 nm (267 km) at 20^{o}N. These data were then extrapolated to a 3^o mesh length on a spherical coordinate system using Bessel's central difference formula, to standardize the spacing of the pressure fields in subsequent derivations. After providing PFEG with several alternate pressure field grids over time, FNMOC currently produces six-hourly fields of surface pressure on a global spherical 1^o mesh (a 180 × 360 grid). The standard west coast six-hourly upwelling indices are a product of the 3^o pressure field interpolated from the global spherical 1^o grid. The monthly indices are derived from a 3^o mesh that is interpolated from the monthly-averages of the six-hourly 1^o pressures. The 3^o mesh for western North American and the Northeast Pacific, and the location of the 15 standard locations, is illustrated in Figure 1.

First derivatives of surface pressure P at each grid point are estimated by taking the difference in pressure between the grid points to either side and dividing by the 6^o angular mesh length (Figure 1 inset).

$$\frac{\delta P}{\delta \phi} \cong \frac{P_{\lambda,\phi+h} - P_{\lambda,\phi-h}}{2h}; \qquad \frac{\delta P}{\delta \lambda} \cong \frac{P_{\lambda+h,\phi} - P_{\lambda-h,\phi}}{2h}; \tag{1}$$

where ϕ and λ are the north and east angular coordinates, respectively, and h is the 3^o mesh length in radians.

The east (u_g) and north (v_g) components of the geostrophic wind are:

$$u_g = -\frac{1}{f\rho_a R}\frac{\delta P}{\delta \phi}; \qquad v_g = +\frac{1}{f\rho_a R cos\phi}\frac{\delta P}{\delta \lambda}; \tag{2}$$

where f is the Coriolis parameter, ρ_a is the density of air (assumed constant at 1.22 kg/m^3), and R is the mean radius of the Earth.

Assuming no friction, the geostrophic wind is parallel to local isobars, with low pressure to the left in the Northern Hemisphere; i.e., wind circulates counter-clockwise (cyclonic) around Northern Hemisphere atmospheric lows. To approximate frictional effects, the geostrophic wind at the sea surface is estimated by rotating the geostrophic wind 15^o to the left and reducing its magnitude by 30%.

Sea surface wind stress is calculated from the geostrophic wind using the classic square-law formula:

$$\vec{\tau} = \rho_a C_d |\vec{v}| \vec{v} \tag{3}$$

where $\vec{\tau}$ is the wind stress vector, ρ_a is the air density, C_d is an empirical drag coefficient, and $\vec{v}$ is the estimated wind vector near the sea surface with magnitude $|\vec{v}|$. A C_d of 0.0013 is used to calculate upwelling from the six-hourly surface pressure fields; the C_d is increased to 0.0026 when the monthly-mean pressure data is used. Nelson (1977) describes in detail why a larger C_d is necessary for the monthly calculations, but basically the monthly averaging of pressure smooths out synoptic atmospheric stability, storm energy, ocean roughness due to waves, etc. (Davidson 1974), as well as observations error. Doubling the C_d is an attempt to account for these differences.

The Ekman transport, $\vec{M}$, is calculated using:

$$\vec{M} = \frac{1}{f} \vec{\tau} \times \vec{k} \tag{4}$$

where $\vec{k}$ is the unit vector directed vertically upward.

The sign of the offshore component of the Ekman transport, $M_x = \tau^y / f$, where x is normal and y parallel to the local coastline orientation, is then reversed to reflect that negative (offshore) Ekman transport leads to positive (upwelling) vertical transport, and positive (onshore) Ekman transport leads to negative (downwelling) vertical transport. The upwelling indices are expressed in units of cubic meters per second per 100 meters of coastline, which is equivalent to metric tons/s/100 m coastline. These values are an index of large-scale coastal upwelling, a mean value representative of mass transport averaged spatially over approximately 200 nautical miles. Small-scale upwelling and downwelling events unresolved by the upwelling indices time and space scales may occur during the averaging period for a particular location.

Caveats

Bakun (1973, 1975) and Mason and Bakun (1986) discuss several caveats for the users of the upwelling indices. As described above, the daily and monthly indices are computed using different C_d values (Equation 3) and are not numerically equivalent. However there is considerable spatial inhomogeneity in the relationship between the daily and monthly series (Bakun 1973). A similar degree of seasonal and interannual variability occurs as well, as seen in the figures in Appendix A. Thus the use of a single adjusted C_d does not completely rectify this discrepancy, and comparisons of these data sets should be done with caution.

The previous reports also point out that the resolution of the gridded pressure fields does not resolve the short correlation scale of the atmosphere near coastal topography.

Bakun (1973) suggests this may lead to artificially high geostrophic winds adjacent to coastal mountain ranges. On a related issue, the distribution of individual pressure observations within an area will not be uniform in space or time, so the available information may misrepresent the true averaged pressure for a grid point at a given time. The patterns and total number of observations will change over time as well, imparting artificial trends or fluctuations in the series.

In addition, at least four different agencies have supplied pressure fields to allow PFEG to construct the 50-year series available today. Differences in the data and methods used by each to produce these fields appear to induce clear changes in the upwelling time series. FNMOC, who currently supplies the pressure fields, has changed the algorithms employed in generating their pressure fields at various times. This also appears to affect the derived indices. These changes should be taken into account when analyzing long-term trends or variations in the upwelling time series.

While the derivations of the indices are based on established theory, they are nonetheless a simplified and incomplete representation of the physics that drive coastal circulation and specifically Ekman transport. Upwelling is due to the combined effect of two processes; coastal upwelling (the process that is the basis of the indices described here) and Ekman pumping (wind curl, or the spatial variation in the wind). The latter process may be an equally important contributor to surface Ekman divergence and upwelling (Bakun and Nelson 1991), thus the reader is cautioned that the data presented here may not represent the true amount of upwelling. In addition, the calculations are based on numerous assumptions and simplified parameterizations, to ease computation and, in some cases, because we can only approximate the true physical world at this point. Future research will no doubt reveal formulations that will improve our representation of coastal dynamics. However the calculations applied in this case do provide a reasonable representation of Ekman transport in the coastal zone, given our current state of knowledge.

Results

A thorough analysis and interpretation of this 50-year record of upwelling indices is beyond the scope of a technical memorandum, but a few details of these data will be highlighted. The reader will find considerable insight from examination of the figures in this report, and we anticipate it will inspire further studies. The daily, weekly and monthly upwelling indices, and their climatologies, are summarized in a series of appendices.

The means and standard deviations of monthly values are calculated for each calendar month for the 25-year period, 1967–91. These are summarized in Figure 3, shown by position in Appendix A, and contoured as a function of time and latitude in

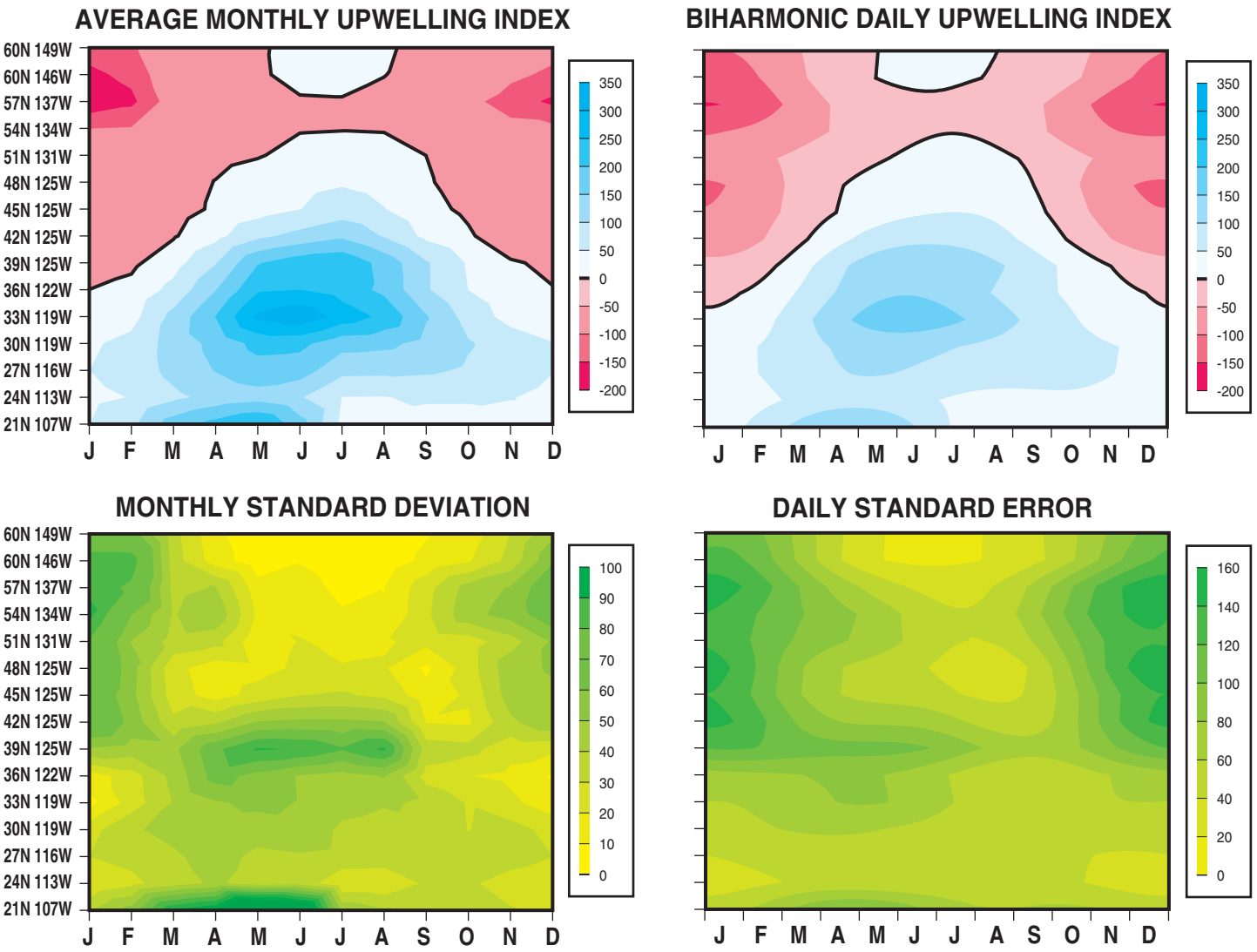

Figure 3. a) Average monthly upwelling index contoured by position and month. Average is for 1967-91. b) Standard deviation of monthly indicies for the same period. c) Biharmonic fit to daily data for 1967-91. d)Standard error of daily indicies for same period. All data contoured by position and time. Dark green values denote higher upwelling values and variance. Units are in $m^3/s/100m$

Appendix C. These values are also used to calculate anomalies from the means of the calendar months (Appendices B, C, and D). Standard anomalies, the anomalies divided by the standard deviation for the calendar month, are contoured in Appendix C.

The upwelling maximum is centered along southern California during summer (Figure 3a). Minima occur at all latitudes in the winter, with negative (downwelling-favorable) means occurring north of 36^{o}N during at least one month of the year. Downwelling is a year-round feature along the British Columbia coast. Times of greatest absolute monthly indices at a location correspond closely with the months of highest interannual variation (Figure 3b). Standard deviations south (north) of 45^{o}N are greatest in summer (winter). The greatest summer variance (ca. 39^{o}N) coincides with the maximum spatial gradient in the mean index, suggesting that interannual shifts in the position of strongest upwelling, rather than in the timing of the upwelling cycle, are responsible for the high standard deviations. The latitude of the highest temporal gradients (33^{o}N) does not have corresponding high standard deviations, further supporting this idea. In contrast, the highest winter deviations do not occur in a region of high spatial or temporal gradients. Thus the more likely explanation for the winter variability is interannual differences in the large-scale subarctic pressure field (e.g., variability in the Aleutian Low), rather than shifts in the timing or position of maximum downwelling wind conditions.

Because the annual upwelling cycle is roughly sinusoidal, the shape of the annual cycle is estimated at each of the 15 grid points by a least-squares regression of the daily data from 1967–91 to an annual and semiannual harmonic signal (Lynn *et al.* 1967; Hayward *et al.* 1995). The biharmonic equation is of the form

$$UI(t) = A_0 + A_1 \cos(2\pi t) + B_1 \sin(2\pi t) + A_2 \cos(4\pi t) + B_2 \sin(4\pi t) \qquad (5)$$

where t is the Julian Day/365 and the A_i and B_i are coefficients determined by the regression for each point, given in Table 1. The fits are not improved significantly by including higher harmonics. Identical 25-year periods were selected for the daily and monthly data to provide an intercomparison of their annual climatologies (Appendix A). Standard errors were calculated for each Julian Day, then fit with the same biharmonic model (Equation 5). The daily harmonic indices and standard errors are contoured as a function of latitude in Figures 3c and 3d, respectively. The biharmonic fits also are regressed against the original 25-year subseries, and against the 25-year subseries that have been low-passed with a Chebychev Type I fifth-order filter with a 30-day cutoff (Table 1). To give an example of the degree of variability in the daily values, the annual biharmonic cycle ± 1 standard error determined at 39^{o}N, 125^{o}W is superimposed on the daily indices from 1967–91 (Figure 4). The last column of Table 1 gives R', the ratio of the variance squared from the unfiltered and low-passed daily fits. Higher values of R'

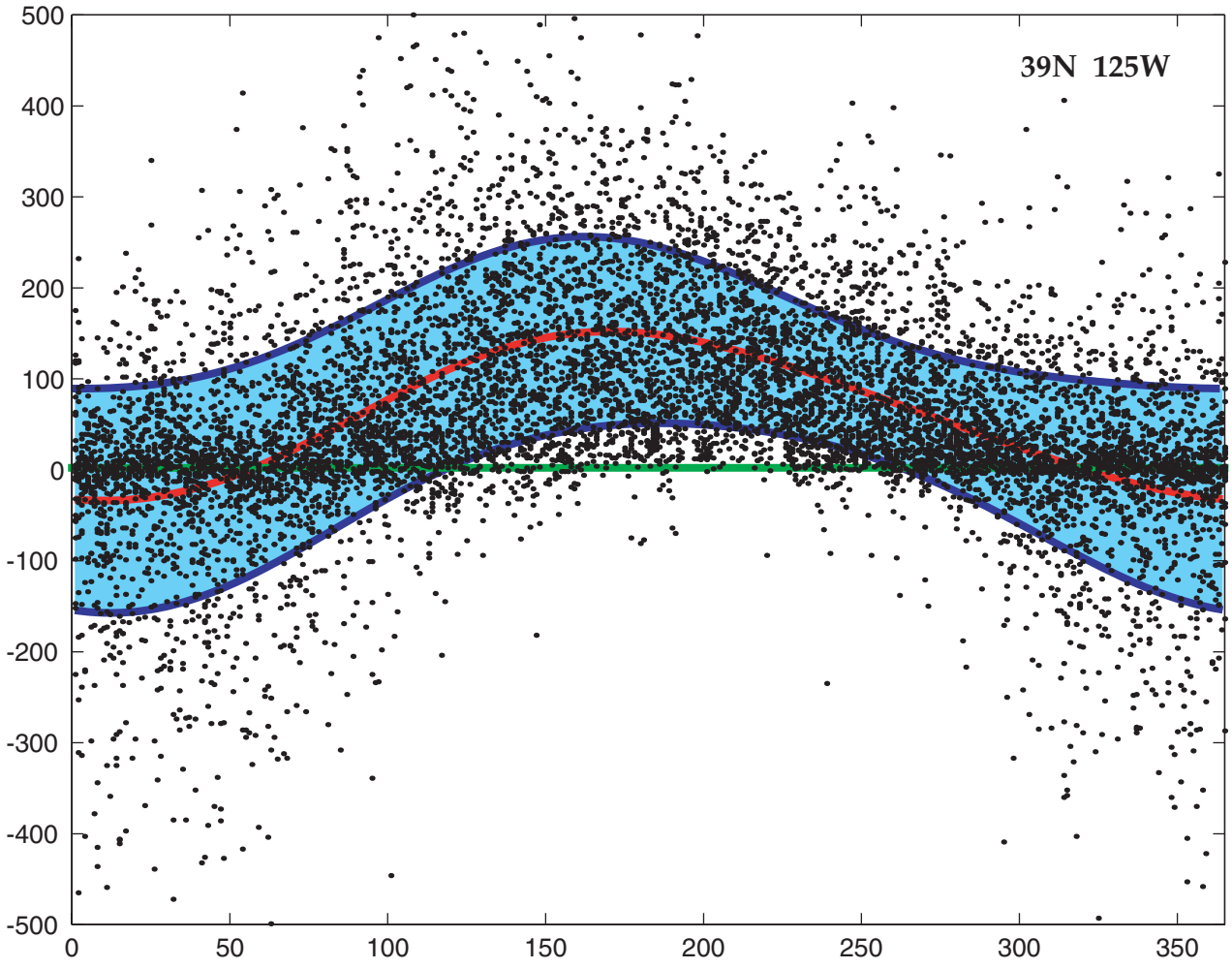

Figure 4. Annual biharmonic fits to daily upwelling indices at 39^{o}N, 125^{o}W (bold curve), +/- one standard error for each Julian Day (shaded area), for period 1967-91. Dots denote individual daily index values for same period. Units are *m^{3}/s/100m*.

denote locations where the amount of high-frequency (synoptic) variance is relatively large compared to low-frequency (interannual) variance.

The characteristics of the annual upwelling cycle at each point, based on the biharmonic fit to the 1967–91 daily values, are summarized in Figure 5. The North American west coast appears to break down into three distinct upwelling regions; Baja California (21–30^{o}N), continental US (30–48^{o}N), and British Columbia and Alaska (48–60^{o}N). The annual range off Baja California is relatively small, with wintertime values of less than 50 $m^3/s/100m$ and summer maxima of 75-150 $m^3/s/100m$. The timing of strongest upwelling increases from late April at 21^{o}N to late May at 30^{o}N. The time of minimum upwelling occurs within about $\pm$15 days of 1 January, a pattern repeated the length of the coast. This region is also characterized by secondary minima and maxima in August and October, respectively (more technically a pair of inflection points in the annual curves at 27^{o}N and 30^{o}N). In contrast, annual cycles north of 30^{o}N have a strong sinusoidal (12-month harmonic) signature. The greatest upwelling rates occur at 33^{o}N, with a linear decrease in the maximum upwelling indices north to about 54^{o}N. The greatest annual range occurs at 39^{o}N. The timing of the maximum continues the appearance of northward propagation, with maximum rates off Oregon and Washington lagging those at 21^{o}N by about 80 days (ca. 25 km/d). Maximum values north of Washington are about zero, and occur in June–July. Minimum indices of about -100 $m^3/s/100m$ occur in ca. 1 January.

The phase of maximum upwelling corresponds with climatological surface conditions along the coast (Lynn 1967). Maximum salinity occurs in May off northern Baja, June-July off southern California, and July and August along central California (ca. 36–38^{o}N). Salinity maxima along southern Baja occur in fall, coinciding with the secondary upwelling maximum. The temperature mimima found by Lynn in upwelling regions, typically in April–May, is impacted substantially by the seasonal surface heat flux and agrees less well with the time of greatest upwelling. The relationship between the annual cycle of upwelling and temperature and salinity is also complicated by advection along the coast, and is influenced by the surface water masses of the California Current.

Annual cycles for the daily and monthly data sets are compared in Figure 3, and in a series of plots in Appendix A. It appears that upwelling indices derived from *monthly* pressure fields overestimate the magnitude of upwelling and downwelling based on monthly averages of the *daily* values. This discrepancy is most evident during the months of the highest absolute values at each location (e.g., monthly indices overestimate winter downwelling at the northern points, and summer upwelling at the southern points). Bakun (1973) discusses the disparity between the daily and monthly indices, and shows the monthly values underestimate the monthly means of the six-hourly Ekman transports by as much as 50%, provided the same value of C_d is

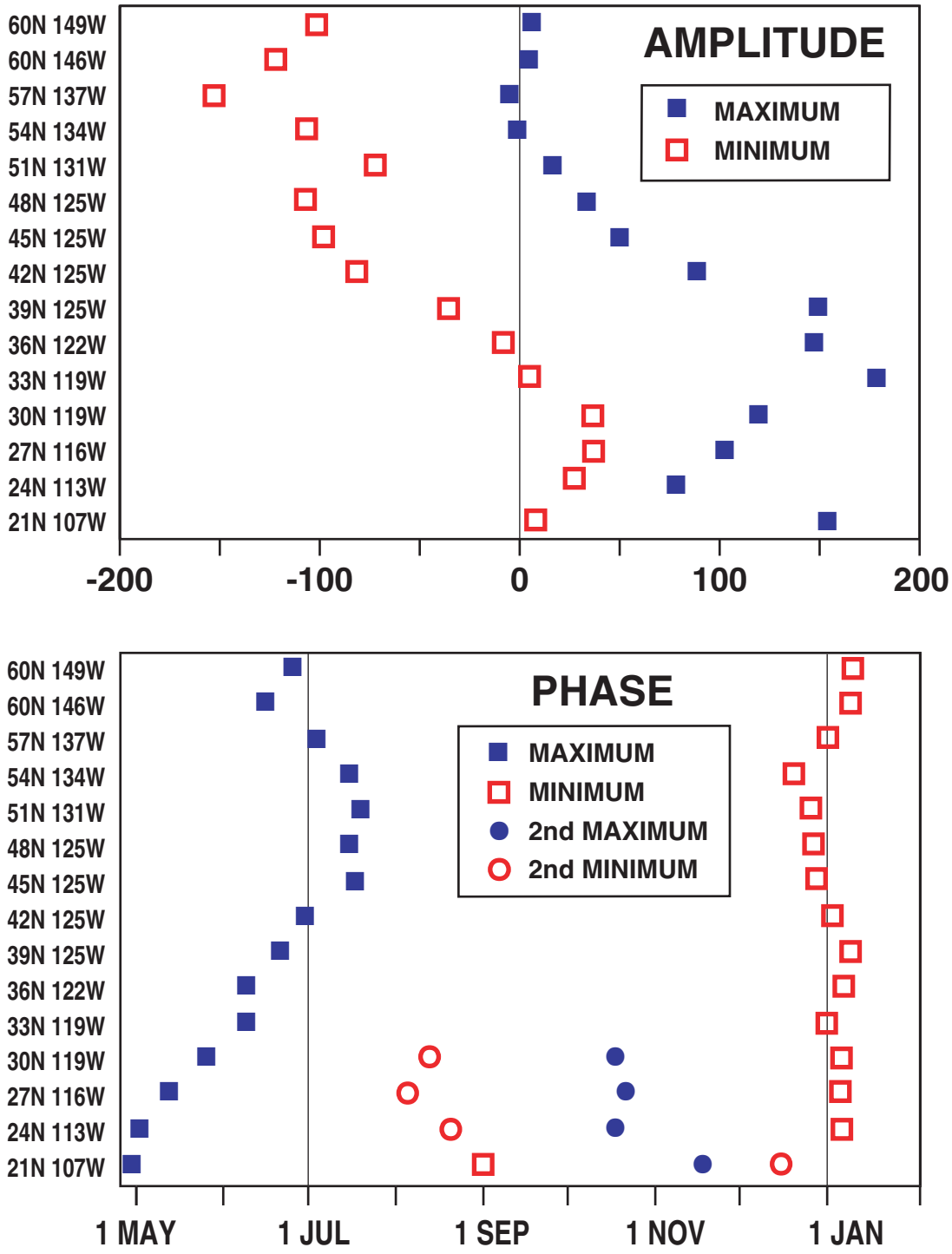

Figure 5. Characteristics of annual cycle of daily upwelling, based on biharmonic fits for period 1967-91. Upper panel shows maximum and minimum amplitudes of annual cycle at each position. Lower panel shows calendar dates of maxima and minima at all locations, and secondary maxima and minima for 21-30^{o}N. Units are $m^3/s/100m$.

used for both (Equation 3). Bakun showed this distortion varies with location as well. Put another way, doubling the C_d in the monthly stress calculations leads to a 130% overestimate of the daily upwelling rates off Alaska, and a factor of two overestimate off southern and Baja California. In addition, Bakun had only 54 months of data available for comparison, so his analysis could not consider whether these differences have a seasonal effect. With 25 years of simultaneous daily and monthly data now available, our preliminary interpretation, as reflected in Figure 3 and Appendix A, is that the relative discrepancy between the two data sets varies with season as well as latitude. We are currently developing a more complete analysis that will hopefully allow the monthly indices to be adjusted temporally and spatially to reflect more realistic estimates of coastal upwelling.

The annual pattern of the daily standard errors separates into geographic regions. Winter conditions are much more variable than summer north of 39^{o}N. Variance is more evenly distributed throughout the year from 24–39^{o}N, with slightly elevated standard errors in spring and a late summer minimum. The seasonal pattern is particularly flat along Baja. The southernmost site is unique in its unusually high variance in late spring, possibly an artifact of changes in the pressure field model used by the Navy.

A comparison between the standard errors of the daily values and the monthly standard deviations reveals some interesting differences (Figure 3). Since $s.e. = s.d./\sqrt{n}$, where n is the sample size, 25 in this case, the standard errors are consistently and substantially greater than the associated monthly deviations. The difference is due to the high degree of variability on a given day associated with synoptic atmospheric motions. These are averaged out in the monthly pressure fields; the monthly deviations reflect large-scale interannual variations while the daily variance is a combination of random storminess in addition to interannual differences. The quantitative differences between these two estimates of variance at a location is therefore an indication of the relative contribution of synoptic and interannual variations. Areas north of 42^{o}N and south of 33^{o}N feature similar annual patterns. Off central and southern California however monthly standard deviations peak in spring and remain relatively high through the summer, while daily standard errors decline rapidly between late winter and summer. This difference is particularly strong at 39^{o}N. Relatively greater wintertime synoptic energy at these latitudes is reflected in the dramatically different annual cycles in daily versus monthly variance. This pattern also agrees with the spatial distribution of R' (Table 1).

The anomalies of the monthly upwelling indices, relative to the 25-year mean of the monthly values for 1967–91, are presented for each location in Appendix B. Means and standard deviations for each calendar month are also given at the bottom of each page.

In Appendix C, plots of the monthly upwelling indices, the monthly anomalies, and the anomalies normalized by the standard deviations for each calendar month are shown. The continuity of anomalies in time and space can be seen in this format The data are broken into five ten-year periods for ease of presentation. The anomalies plotted here are given in the tables in Appendix B. One of the most striking highlights of these figures is the relatively short duration of significant positive and negative anomalies, despite the large spatial extent of most of the anomalies. Strong ENSO events (e.g., 1957, 1983, 1992) correspond to significant negative anomalies along much of the U.S. coast. Positive and negative upwelling anomalies correspond closely to cool and warm coastal SST anomalies, respectively, calculated by Cole and McLain (1989) for the period 1971–87, suggesting that SST interannual variability is related to differences in coastal upwelling, which is approximated reasonably well by these indices.

Anomalies of monthly upwelling indices, as given in Appendix B, are plotted as 50-year time series for each location in Appendix D. Again the short duration of large anomalies (typically a few months) is apparent. These time series also display the spatial coherence of many of the anomalies. These series also feature sudden shifts in the temporal pattern of the indices. One example is the relatively poor fit of the annual mean prior to 1955 off southern California, reflected in the apparently large annual signal in the anomalies. Another example is the dramatic change in 1976 at 21^oN, which is due to a shift in the summer indices. These changes are also apparent in the anomalies in Appendix B and in the contour plots in Appendix C. These changes in the patterns of the indices are questionable, and may be attributed to changes in the source of the monthly pressure fields (Bakun 1973), or in the methodology used to interpolate the gridded pressure fields used to calculate these indices.

The final set of figures (Appendix E) contains a series of plots, by year, of daily and weekly-averaged upwelling indices for 1986–1995. Superimposed on each figure is the annual biharmonic fit to the daily indices for that location. The shaded area covers $\pm$ one standard error from the mean. Periods of anomalously strong and weak upwelling and downwelling, typically on the time scales of storms and other atmospheric events, can be quickly identified in these figures as outliers from the standard error envelope. The plots are separated by location.

Modernization

Rapid advancements in computing and communications since the initial development of the upwelling index over two decades ago have led to more accurate and efficient calculation and distribution of the products described here. Several factors contribute to improved data quality and more timely distribution. Collection of surface pressure data is now more routine and the oceans are now covered more completely with observations

than in the past. Models employed by the Navy to interpolate the gridded fields from observations have been improved. High-speed desktop computers, high-resolution printers, and modern graphics software are now available to produce the data products efficiently, economically and with much higher quality. Finally, new telecommunication methods and procedures such as e-mail, file transfer protocol (ftp), and the Internet, allow large volumes of data and model output to be transferred between computers, stored more efficiently and securely, and processed in a more portable fashion. Hard copy delivery is rapidly giving way to electronic transmission of the upwelling indices and products, which provides scientists and managers much quicker access to information than in the past. Within the next year, we envision having the upwelling indices and many other PFEG data products available on our world-wide web home page (*http:/www.pfeg.noaa.gov*). This will make information easily accessible to a wider spectrum of users as soon as it is generated.

We are also looking at ways to improve the value of the upwelling index. First, differences between the daily and monthly indices as a function of time and location are being analyzed in greater detail, which will allow the monthly indices to be adjusted to represent coastal upwelling rates more realistically. Alternative derivations of upwelling are being evaluated (e.g., including frictional effects and the role of wind curl). While these factors may be less critical at the standard points summarized here, such modifications certainly will be important in other ocean regions. Other analyses are relating the upwelling index time series to series based on measured winds, as well as other environmental variables that represent upwelling (e.g., coastal sea level, SST). This will lead to a better understanding of how well the indices actually represent coastal upwelling. Finally, we will continue to interact with researchers using the indices to link environmental and fisheries variability, to learn where these series may not be biologically relevant and, more generally, what type of information may be most useful to them. All these improvements will contribute to the long-term goal of producing an environmental index that has greater utility for biologists, fisheries scientists and resource managers.

While the upwelling indices described here are by far the most popular product that PFEG derives from the surface pressure fields, they are but one of several atmospheric and oceanic products presently generated from the six-hourly pressures. The following derived fields are currently available from PFEG for the 15 standard points and the entire North Pacific and Atlantic Oceans on 3^o and 5^o grids:

SEA LEVEL PRESSURE
SURFACE GEOSTROPHIC WIND VECTOR (east and north components)
SURFACE WIND STRESS VECTOR (east and north components)
CURL OF WIND STRESS

CUBE OF WIND SPEED
EKMAN TRANSPORT VECTOR (east and north components)
OFFSHORE EKMAN TRANSPORT COMPONENT
DIRECTON OF OFFSHORE EKMAN TRANSPORT COMPONENT
VERTICAL VELOCITY INTO EKMAN LAYER
SVERDRUP TRANSPORT

In addition, the following fields are generated for the entire North Pacific:

TOTAL SURFACE TRANSPORT (east and north components)
TOTAL INTEGRATED TRANSPORT
INTEGRATED GEOSTROPHIC TRANSPORT

While all of these fields are based on fundamental physical theory, most have not been analyzed nor applied to scientific problems. It is our hope to conduct a critical analysis of these other products and promote their use by researchers and managers. A future technical memorandum is planned that will summarize some of the more important products. In the interim, they are available to interested parties, and we encourage their use.

Acknowledgments

The upwelling indices are a product of years of development and improvement by scores of individuals. We are indebted to Andrew Bakun for originally developing the upwelling index, commonly referred to as the Bakun index. James Johnson, Gunter Seckel, and Douglas McLain provided advice in its initial development. David Husby, Craig Nelson, Richard Parrish, Roy Mendelssohn, Jerrold Norton, Arthur Stroud, and George Boehlert are among our many former and current colleagues at PFEG who contributed advice, stimulating discussion and valuable information, and suggested improvements. David Cole, Christie Johnson Sharp, and Heather Parker are acknowledged for their efforts in producing and distributing these indices each month. Tone Nichols is particularly recognized for generating most of the graphics and for her technical support. David VenTresca (California Department of Fish and Game, Monterey) and Ronald Lynn (NMFS Southwest Fisheries Science Center, La Jolla) graciously reviewed this manuscript. Analyzed digital atmospheric pressure data, computing and graphical facilities, and considerable logistical support were provided by U.S. Navy, Fleet Numerical Meteorology and Oceanography Center. Finally, we are grateful to the many scientists who have applied the indices in their research, and have given us valuable suggestions for their improvement.

References

Ainley, D.G., W.J. Sydeman, R.H. Parrish, and W.H. Lenarz. 1993. Oceanic factors influencing occurrence patterns of young rockfish *Sebastes* in central California: a predator's perspective. *Calif. Coop. Oceanic Fish. Invest. Rep. 34*:133-139.

Ainley, D.G., W.J. Sydeman, and J. Norton. 1995. Upper trophic level predators indicate interannual negative and positive anomalies in the California Current food web. *Mar. Ecol. Prog. Ser. 118*:69-79.

Bakun, A. 1973. Coastal upwelling indices, west coast of North America, 1946-71. U.S. Dep. Commer., NOAA Tech. Rep., NMFS SSRF-671, 103 p.

Bakun, A. 1975. Daily and weekly upwelling indices, west coast of North America, 1967-73. U.S. Dep. Commer., NOAA Tech. Rep., NMFS SSRF-693, 114 p.

Bakun, A. 1990. Global climate change and intensification of coastal ocean upwelling. *Science 247*:198-201.

Bakun, A. and C.S. Nelson. 1977. Climatology of upwelling related processes off Baja California. *Calif. Coop. Oceanic Fish. Invest. Rep. 19*: 107-127.

Bakun, A. and C.S. Nelson. 1991. The seasonal cycle of wind-stress curl in subtropical eastern boundary current regions. *J. Phys. Oceanogr.* **21**:1815-1834.

Brodeur, R.D. and D.M. Ware. 1992. Long-term variability in zooplankton biomass in the subarctic Pacific Ocean. *Fish. Oceanogr. 1*:32-38.

Botsford, L.W. and D.E. Wickham. 1975. Correlation of upwelling index and Dungeness crab catch. *Fish. Bull. 73*:901-907.

Cole, D.A. and D.R. McLain. 1989. Interannual variability of temperature in the upper layer of the north Pacific eastern boundary region, 1971-1987. U.S. Dep. Commer., NOAA Tech. Rep., NOAA-TM-NMFS-SWFC-125, 9 p. + figs.

Cury, P. and C. Roy. 1989. Optimal environmental window and pelagic fish recruitment success in upwelling areas. *Can. J. Fish. Aquat. Sci. 46*:670-680.

Cury, P., C. Roy, R. Mendelssohn, A. Bakun, D.M. Husby, and R.H. Parrish. 1995. Moderate is better: exploring nonlinear climatic effects on the Californian northern anchovy (*Engraulis mordax*). In R.J. Beamish (ed.), Climate Change and Northern Fish Populations. *Can. Spec. Publ. Fish. Aquat. Sci. 121*, p. 417-424.

Cushing, D.H. 1969. Upwelling and fish production. FAO Fish. Tech. Paper 84. 40 p.

Davidson, K.L. 1974. Observational results on the influence of stability and wind-wave coupling on momentum transfer and turbulent fluctuations over ocean waves. *Boundary-Layer Met. 6*:305-331.

Ekman, V.W. 1905. On the influence of the earth's rotation on ocean currents. *Ark. Mat. Astron. Fys. 2*(11):1-52.

Fisher, J.P. and W.G. Pearcy. 1988. Growth of juvenile coho salmon (*Oncorhynchus*

kisutch) off Oregon and Washington, USA, in years of differing coastal upwelling. *Can. J. Fish. Aquat. Sci. 45*:1036-1044.

Hayward, T., D. Cayan, P. Franks, R. Lynn, A. Mantyla, J. McGowan, P. Smith, F. Schwing and E. Venrick. 1995. The state of the California Current in 1994-1995: a period of transition. *Calif. Coop. Oceanic Fish. Invest. Rep. 36*: 19-39.

Hiss, J.M. 1995. Environmental Factors Influencing Spawning Escapement of Dungeness River pink salmon (*Oncorhynchus gorbuscha*) 1959-1993. USFWS, Western Washington Fishery Resource Office, Olympia, WA. 50 p.

Huyer, A. 1983. Coastal upwelling in the California Current. *Prog. Oceanogr. 12*:259-284.

Huyer, A. and R.L. Smith. 1985. The signature of El Niño off Oregon, 1982-1983. *J. Geophys. Res. 90*:7133-7142.

Kosro, P.M., A. Huyer, S.R. Ramp, R.L. Smith, F.P. Chavez, T.J. Cowles, M.P. Abbott, P.T. Strub, R.T. Barber, P. Jessen, and L.F. Small. 1991. The structure of the transition zone between coastal waters and the open ocean off northern California, winter and summer 1987. *J. Geophys. Res. 96*:14707-14730.

Lynn, R.J. 1967. Seasonal variation of temperature and salinity at 10 meters in the California Current. *Calif. Coop. Oceanic Fish. Invest. Rep. 11*:157-186.

Mason, J.E. and A. Bakun. 1986. Upwelling index update, U.S. west coast, 33N-48N latitude. U.S. Dep. Commer., NOAA Tech. Memo., NOAA-TM-NMFS-SWFC-67, 81 p.

McConnaughey, R.A., D.A. Armstrong, B.M. Hickey, and D.R. Gunderson. 1992. Juvenile Dungeness crab (*Cancer magister*) recruitment variability and oceanic transport during the pelagic larval phase. *Can. J. Fish. Aquat. Sci. 49*:2028-2044.

Nelson, C.S. 1977. Wind stress and wind-stress curl over the California Current. U.S. Dep. Commer., NOAA Tech. Rep., NMFS SSRF-714, 87 p.

Nickelson, T.E. 1986. Influences of upwelling, ocean temperature, and smolt abundance on marine survival of coho salmon (*Oncorhynchus kisutch*) in the Oregon Production Area. *Can. J. Fish. Aquat. Sci. 43*:527-535.

Parrish, R.H., C.S. Nelson, and A. Bakun. 1981. Transport mechanisms and reproductive success of fishes in the California Current. *Biol. Oceanogr. 1*:175-203.

Parrish, R.H. and A.D. MacCall. 1978. Climate variation and exploitation in the Pacific mackerel fishery. Cal. Dep. Fish and Game, Fish Bull. 167. 110 pp.

Parrish, R.H. and D.L. Mallicoate. 1995. Variation in the condition factors of California pelagic fishes and associated environmental factors. *Fish. Oceanogr. 4*:171-190.

Peterson, W.T. and C.B. Miller. 1977. Seasonal cycle of zooplankton abundance and species composition along central Oregon coast. *Fish. Bull. 75*:717-724.

Robinson, M.K. 1976. Atlas of North Pacific Ocean: monthly mean temperatures and mean salinities of the surface layer. Ref. Publ. 2, Naval Oceanographic Office, Washington, DC. 173 p.

Ryther, J.H. 1969. Photosynthesis and fish production in the sea. *Science 166*:72-76.

Smith, R.L. 1968. Upwelling. *Oceanogr. Mar. Biol. Ann. Rev. 6*:11-46.

Sverdrup, H.U., M.W. Johnson, and R.H. Fleming. 1942. The oceans, their physics, chemistry, and general biology. Prentice-Hall, New York, 1087 p.

Thomson, R.E. and D.M. Ware. 1996. A current index of ocean variability. *J. Geophys. Res. 101*:14297-14310.

Traganza, E.D., J.C. Conrad, and L.C. Breaker. 1981. Satellite observations of a cyclonic upwelling system and giant plume in the California Current. In F.A. Richards (ed.), Coastal Upwelling, Amer. Geophys. Union, Washington, DC. p. 228-241.

van Geen, A. and D.M. Husby. 1996. Cadmium in the California Current system: tracer of past and present upwelling. *J. Geophys. Res. 101*:3489-3507.

VenTresca, D.A., R.H. Parrish, J.L. Houk, M.L. Gingras, S.D. Short, and N.L. Crane. 1995. El Niño effects on the somatic and reproductive condition of blue rockfish, *Sebastes mystinus*. *Calif. Coop. Oceanic Fish. Invest. Rep. 36*:167-174.

Walsh, J.J., T.E. Whitledge, J.C. Kelley, S.A. Huntsman, and R.D. Pillsbury. 1977. Further transition states of the Baja California upwelling system. *Limnol. Oceanogr. 22*:264-280.

Wroblewski, J.S. 1977. A model of phytoplankton plume formation during variable Oregon upwelling. *J. Mar. Res. 35*:357-394.

Wooster, W.S. and J.L. Reid, Jr. 1963. Eastern Boundary Currents. p. 253-280. In M.N. Hill (ed.), The Sea, Vol. 2. Interscience, New York. 554 p.

This manuscript was prepared with the AGU LaTeX macros v3.1.

APPENDIX A - ANNUAL CYCLES OF DAILY AND MONTHLY UPWELLING INDICES

The following five pages show the annual cycle of upwelling at the 15 standard locations. The diamonds denote the mean of the **monthly** upwelling indices for each calendar month for the period 1967–91. The vertical bars denote ± one standard deviation for each calendar month. The bold curve is a biharmonic fit to the **daily** upwelling indices for the period 1967–91, estimated by a least-squares regression of the daily data to an annual and semiannual harmonic signal (Equation 5). The shaded area around the biharmonic curve denotes ± one standard error, calculated for each Julian Day. Three locations are shown on each page, from north to south.

The units are metric tons per second per 100 m of coastline (or equivalently cubic meters per second per 100 meters of coastline). These units may be thought of as the average amount (in metric tons or cubic meters) of water upwelled through the bottom of the Ekman layer each second along each 100 m of a straight line directed along the dominant trend of the coast on a scale of about 200 miles. Because of uncertainties in some of the constants employed, and for other reasons outlined in this and the previous three related NOAA Technical Memoranda, these indices should be considered as indicative of short-term relative fluctuations at a location rather than as quantitative measures of absolute magnitude.

DAILY & MONTHLY UPWELLING INDICES
ANNUAL CYCLES

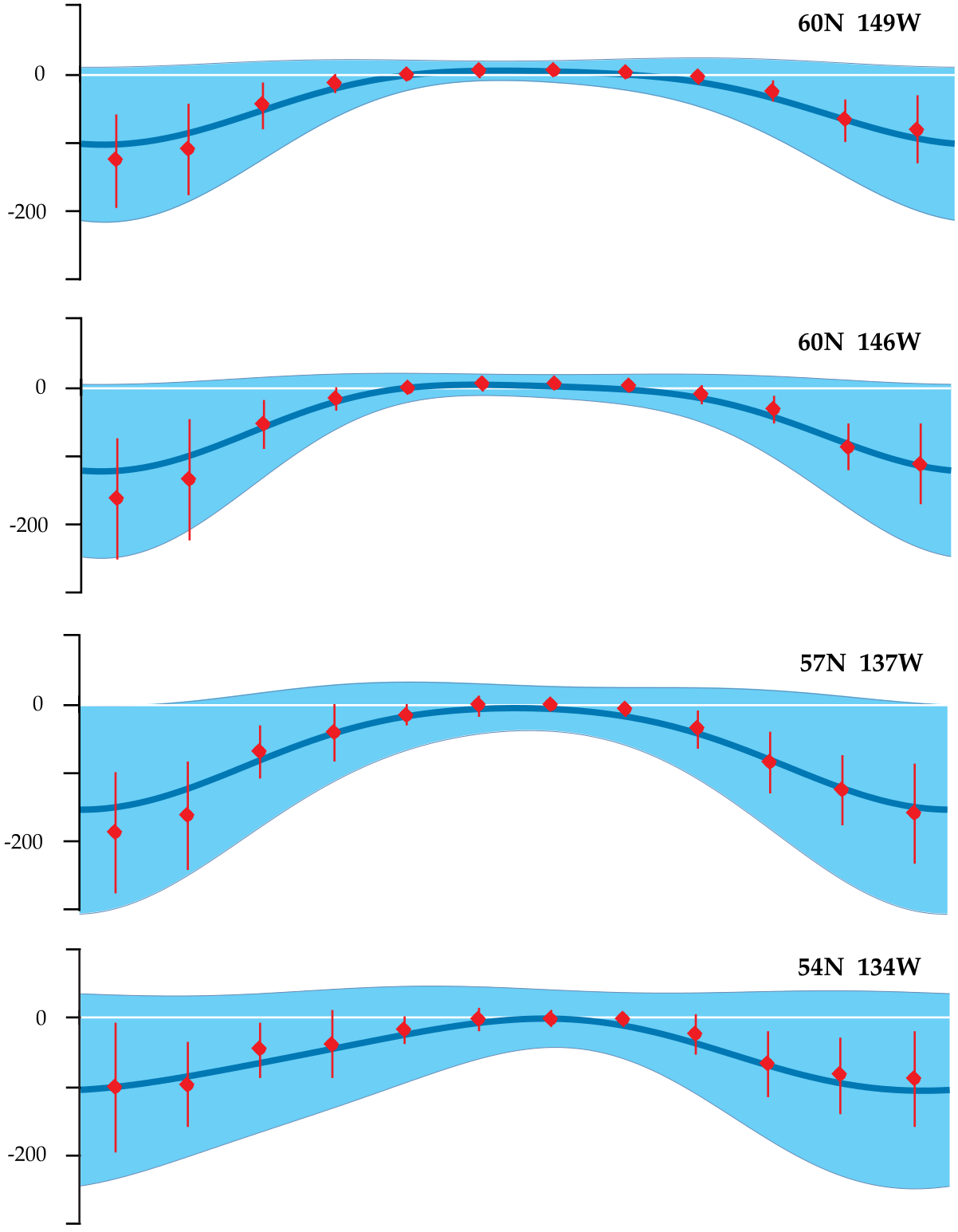

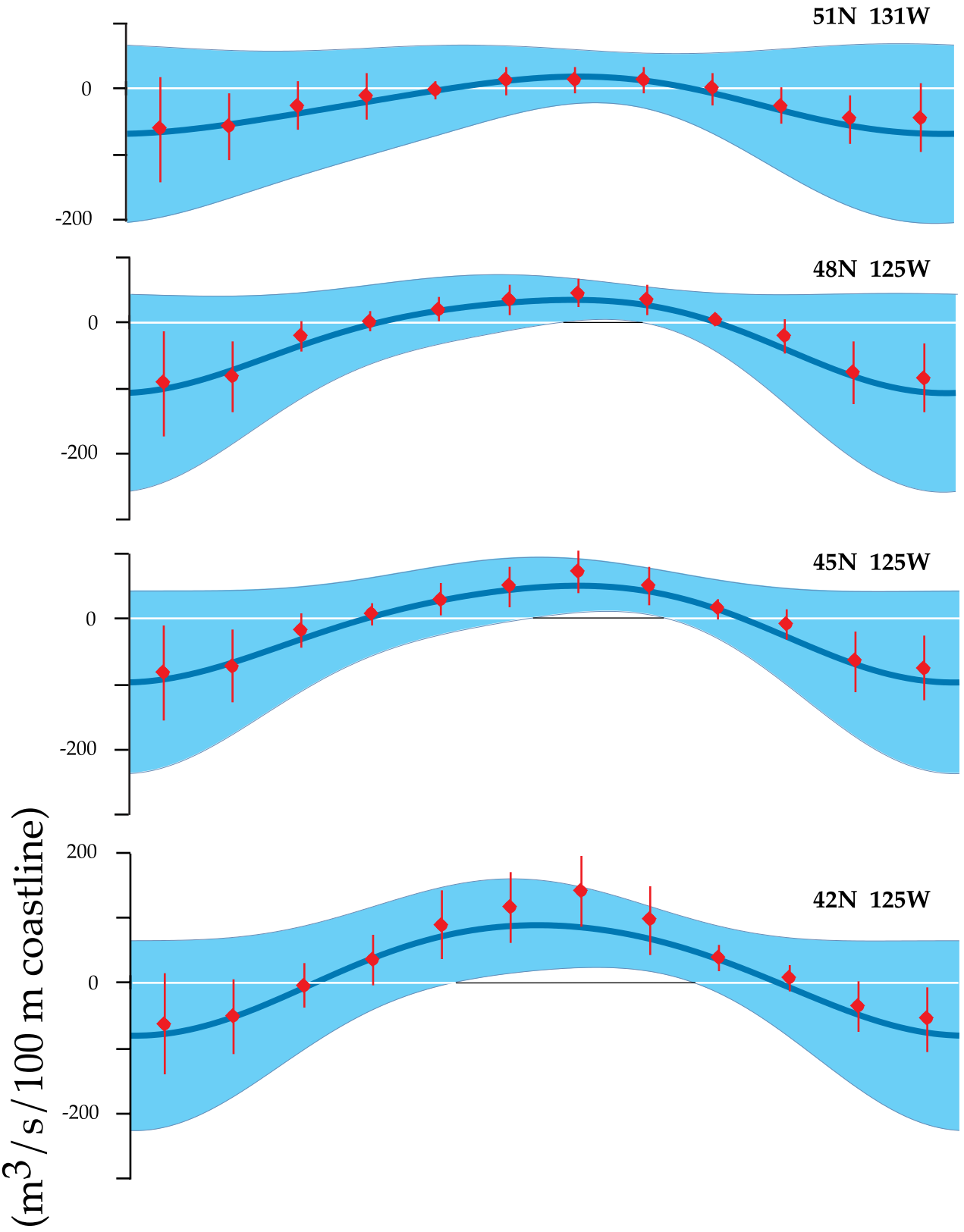
51N 131W
48N 125W
45N 125W
42N 125W
200
0
-200
(m3/s/100 m coastline)

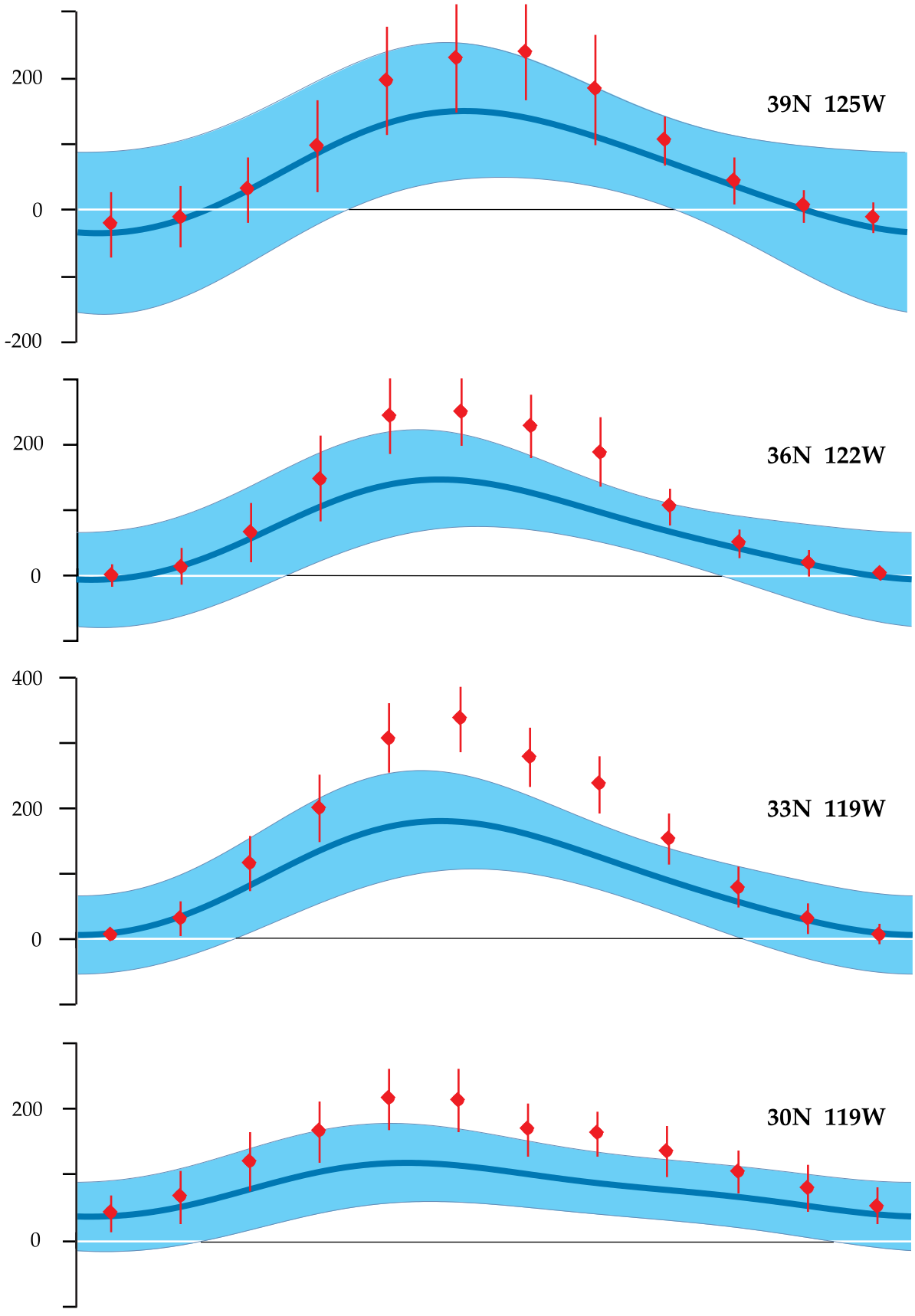
200
0
-200
39N 125W
200
0
36N 122W
400
200
0
33N 119W
200
0
30N 119W

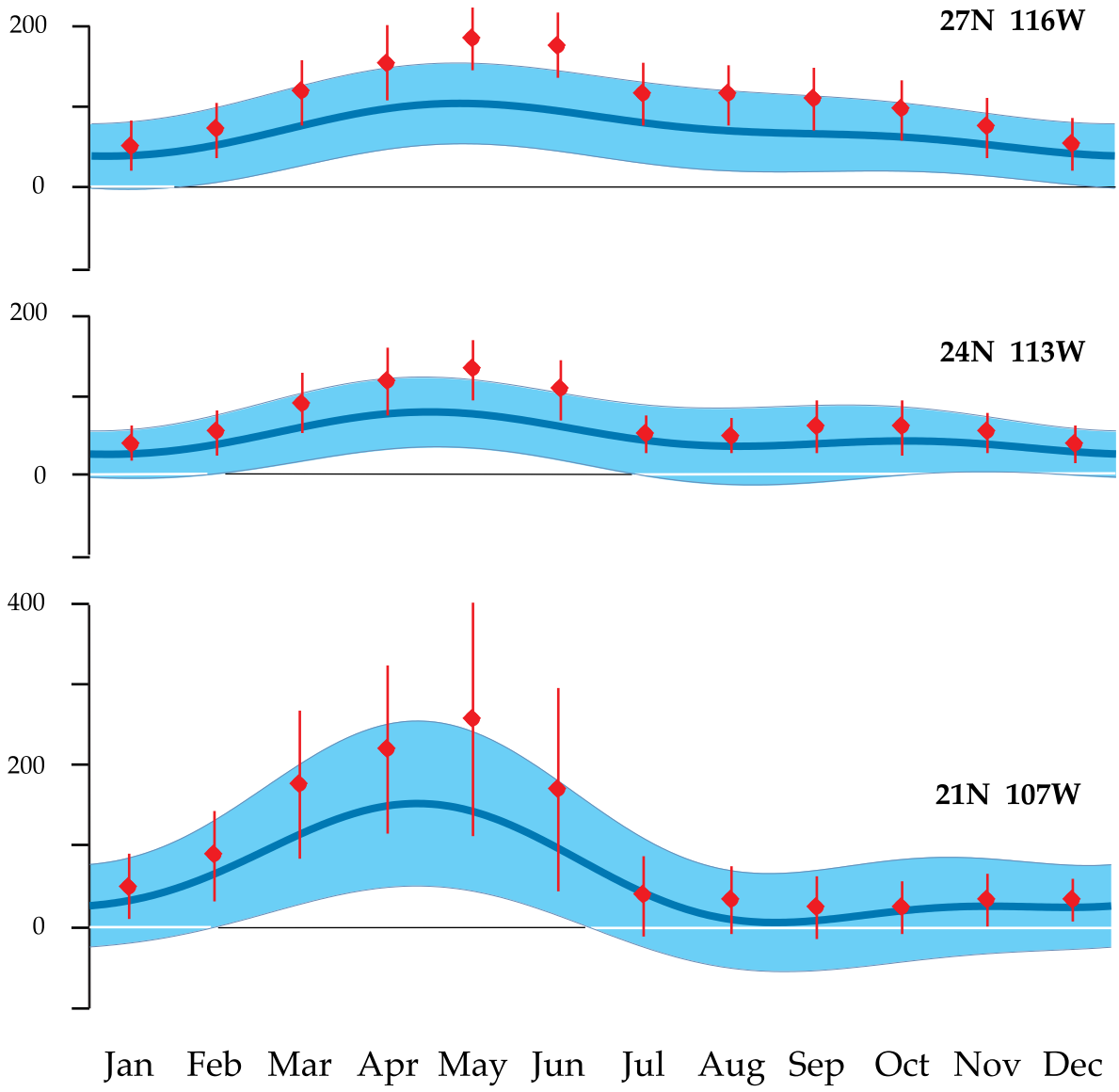
27N 116W
200
0
24N 113W
200
0
21N 107W
400
200
0
Jan
Feb
Mar
Apr
May
Jun
Jul
Aug
Sep
Oct
Nov
Dec

APPENDIX C - MONTHLY UPWELLING INDICES, ANOMALIES AND STANDARDIZED ANOMALIES

The following five pages contain contours of the monthly upwelling indices, the monthly anomalies, and the standard anomalies for each calendar month. The data are contoured with time (in months) as the abscissa and latitude as the ordinate. The anomalies are relative to the 25-year mean of the monthly values in each month for the period 1967–91, and the standard anomalies are the anomalies divided by the standard deviation for the calendar month. The monthly values are shaded, with darker shading representing negative (downwelling) indices. The contour interval for the monthly values is 100 cubic meters per second per 100 m of coastline. Negative anomalies are shaded. The contour interval for the anomalies is 50 cubic meters per second per 100 m of coastline. Monthly standardized anomalies greater than one, that is anomalies greater than one standard deviation from the 25-year mean, are denoted with light shading. Monthly standardized anomalies less than -1 are denoted with dark shading. The data are broken into five ten-year periods for ease of presentation.

The units are metric tons per second per 100 m of coastline (or equivalently cubic meters per second per 100 meters of coastline). These units may be thought of as the average amount (in metric tons or cubic meters) of water upwelled through the bottom of the Ekman layer each second along each 100 m of a straight line directed along the dominant trend of the coast on a scale of about 200 miles. Because of uncertainties in some of the constants employed, and for other reasons outlined in this and the previous three related NOAA Technical Memoranda, these indices should be considered as indicative of short-term relative fluctuations at a location rather than as quantitative measures of absolute magnitude.

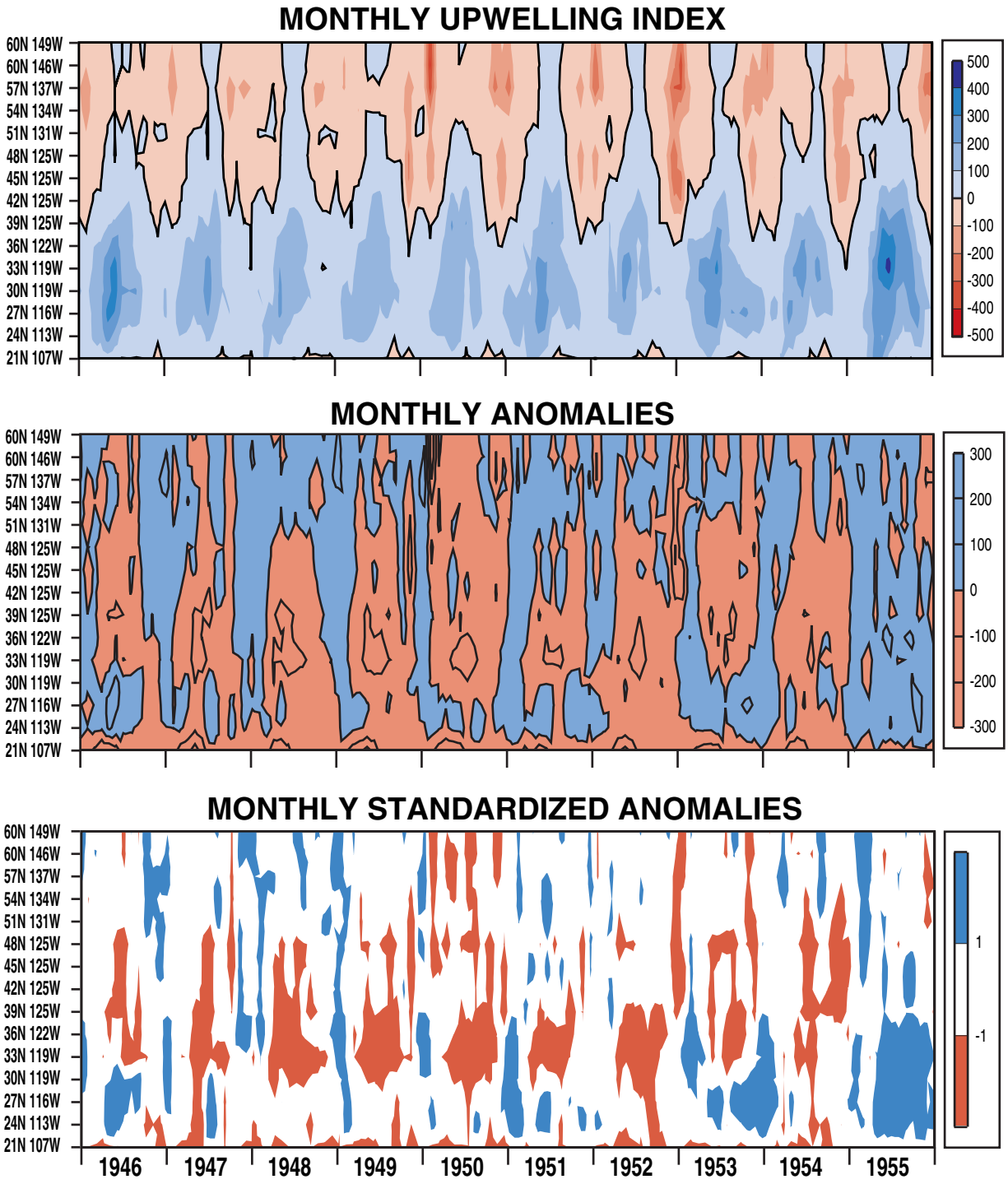
MONTHLY UPWELLING INDEX
60N 149W
60N 146W
57N 137W
54N 134W
51N 131W
48N 125W
45N 125W
42N 125W
39N 125W
36N 122W
33N 119W
30N 119W
27N 116W
24N 113W
21N 107W
500
400
300
200
100
0
-100
-200
-300
-400
-500
MONTHLY ANOMALIES
60N 149W
60N 146W
57N 137W
54N 134W
51N 131W
48N 125W
45N 125W
42N 125W
39N 125W
36N 122W
33N 119W
30N 119W
27N 116W
24N 113W
21N 107W
300
200
100
0
-100
-200
-300
MONTHLY STANDARDIZED ANOMALIES
60N 149W
60N 146W
57N 137W
54N 134W
51N 131W
48N 125W
45N 125W
42N 125W
39N 125W
36N 122W
33N 119W
30N 119W
27N 116W
24N 113W
21N 107W
1
-1
1946
1947
1948
1949
1950
1951
1952
1953
1954
1955

MONTHLY UPWELLING INDEX

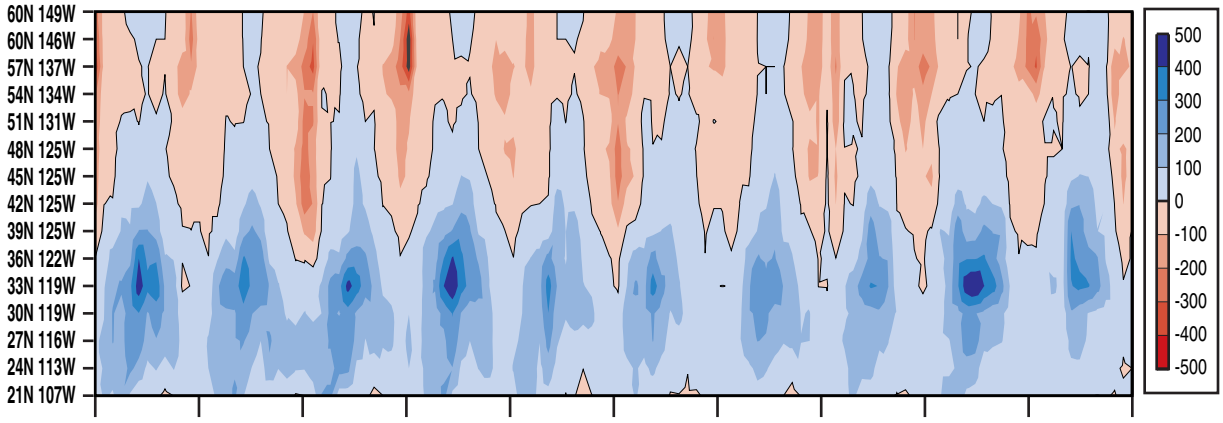

MONTHLY ANOMALIES

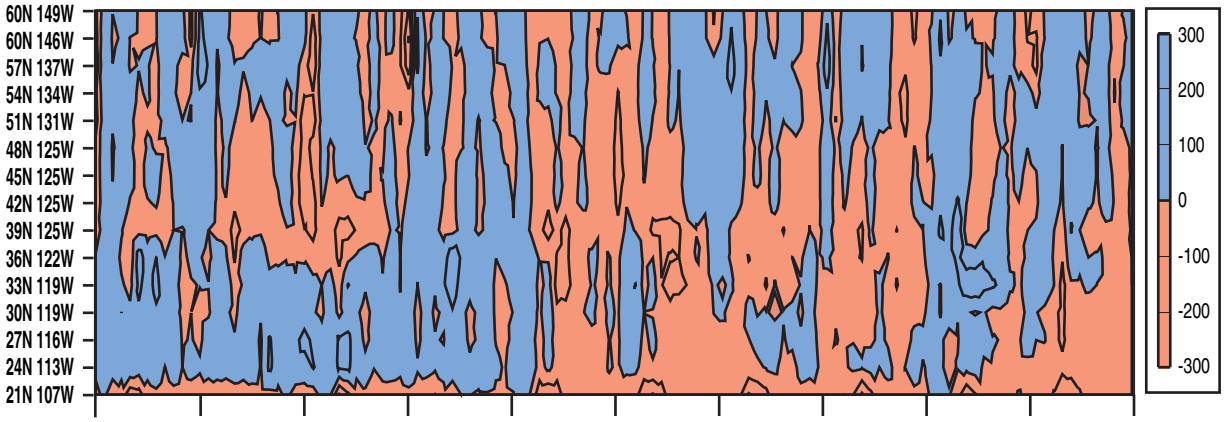

MONTHLY STANDARDIZED ANOMALIES

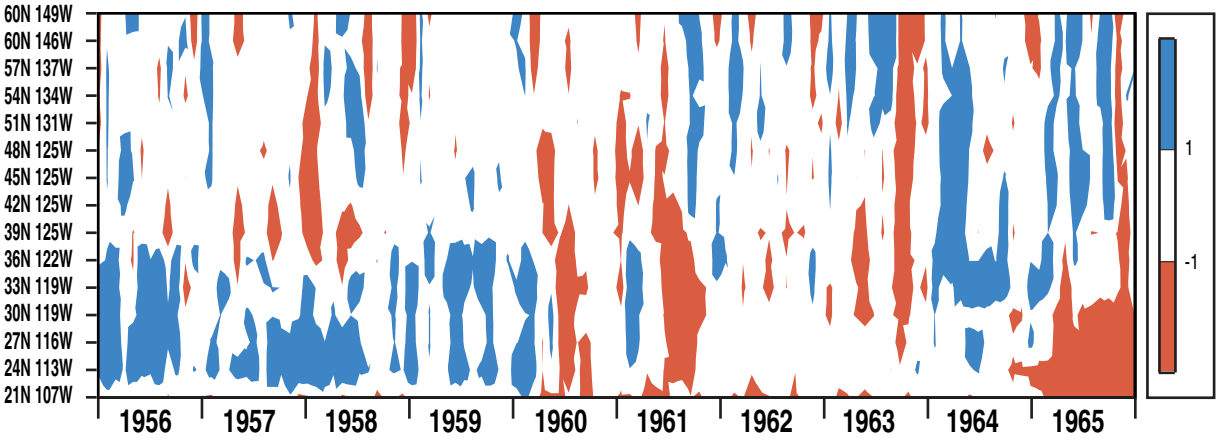

MONTHLY UPWELLING INDEX

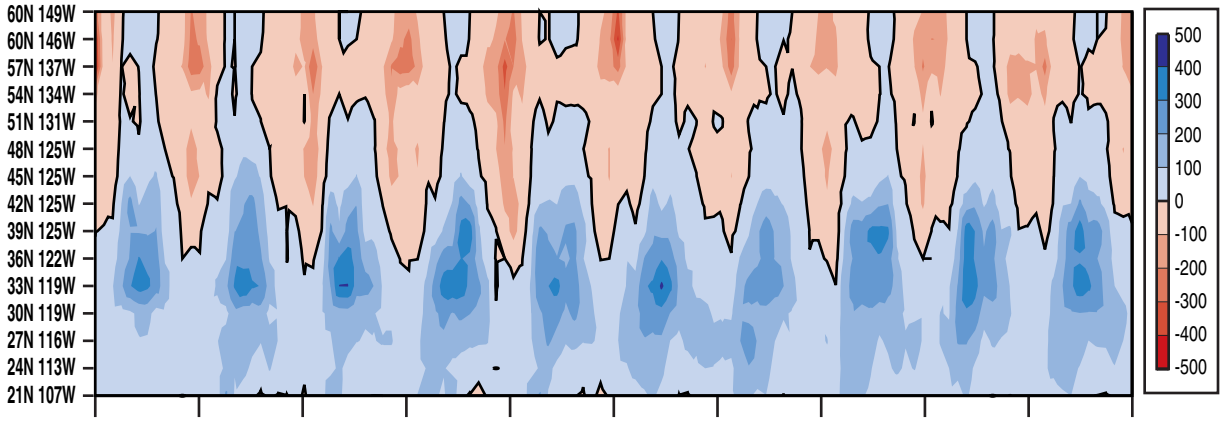

MONTHLY ANOMALIES

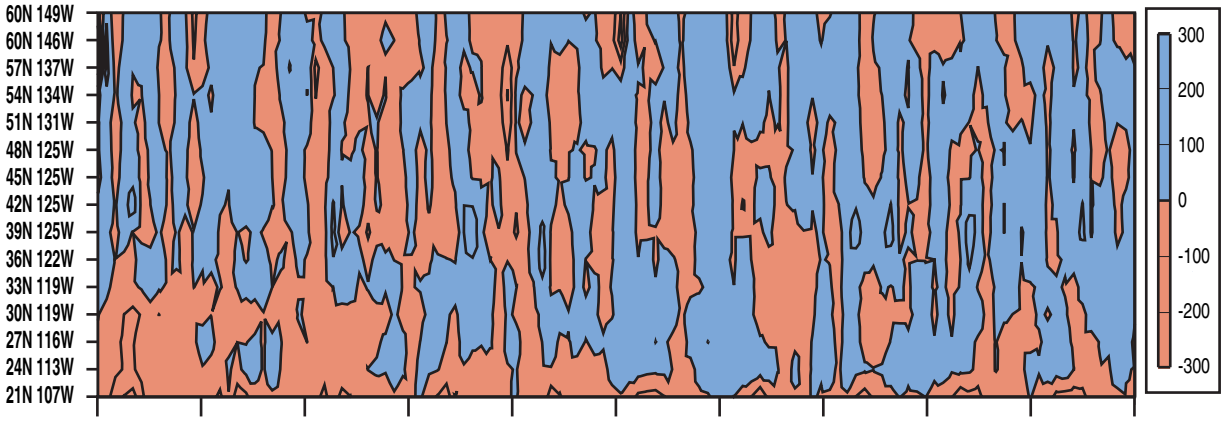

MONTHLY STANDARDIZED ANOMALIES

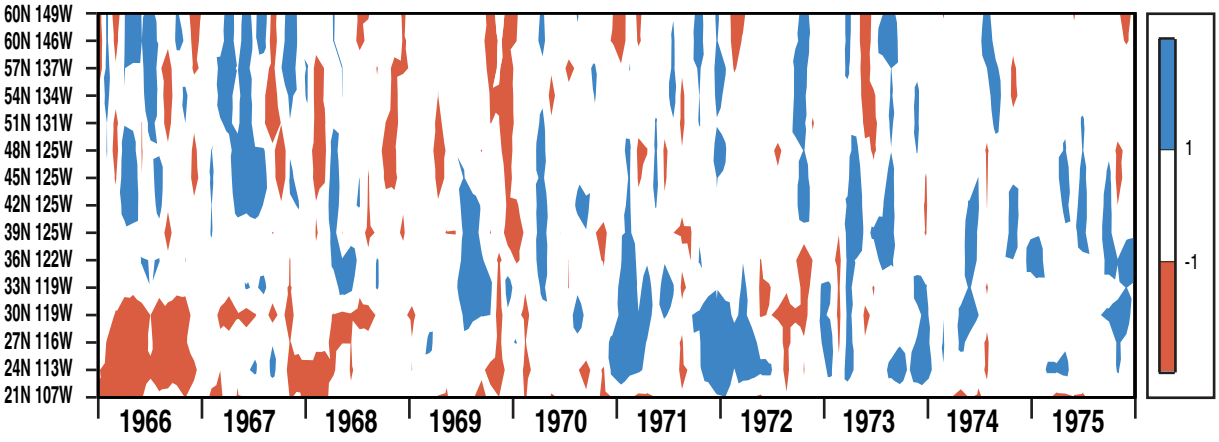

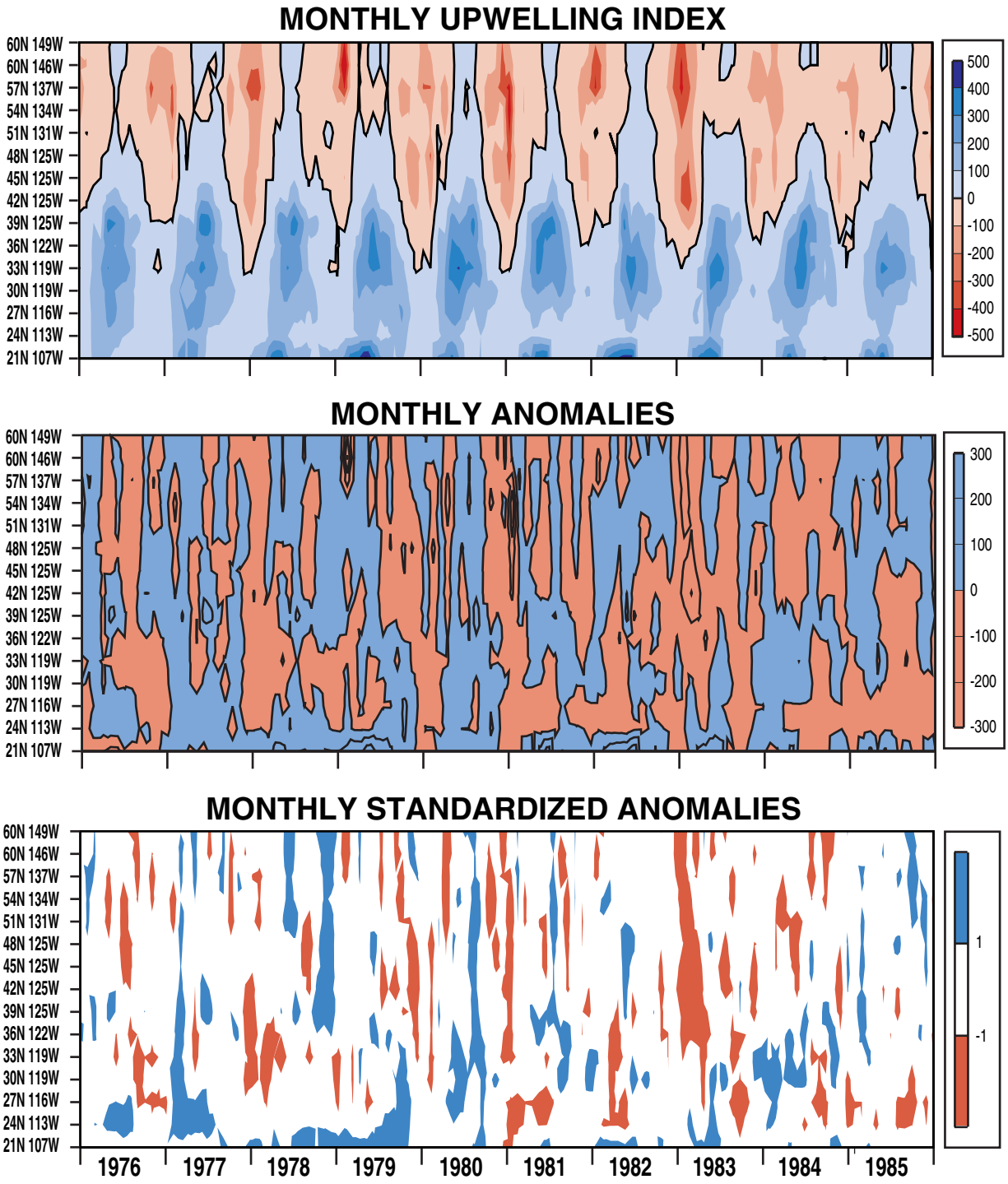
MONTHLY UPWELLING INDEX
60N 149W
60N 146W
57N 137W
54N 134W
51N 131W
48N 125W
45N 125W
42N 125W
39N 125W
36N 122W
33N 119W
30N 119W
27N 116W
24N 113W
21N 107W
500
400
300
200
100
0
-100
-200
-300
-400
-500
MONTHLY ANOMALIES
60N 149W
60N 146W
57N 137W
54N 134W
51N 131W
48N 125W
45N 125W
42N 125W
39N 125W
36N 122W
33N 119W
30N 119W
27N 116W
24N 113W
21N 107W
300
200
100
0
-100
-200
-300
MONTHLY STANDARDIZED ANOMALIES
60N 149W
60N 146W
57N 137W
54N 134W
51N 131W
48N 125W
45N 125W
42N 125W
39N 125W
36N 122W
33N 119W
30N 119W
27N 116W
24N 113W
21N 107W
1
-1
1976
1977
1978
1979
1980
1981
1982
1983
1984
1985

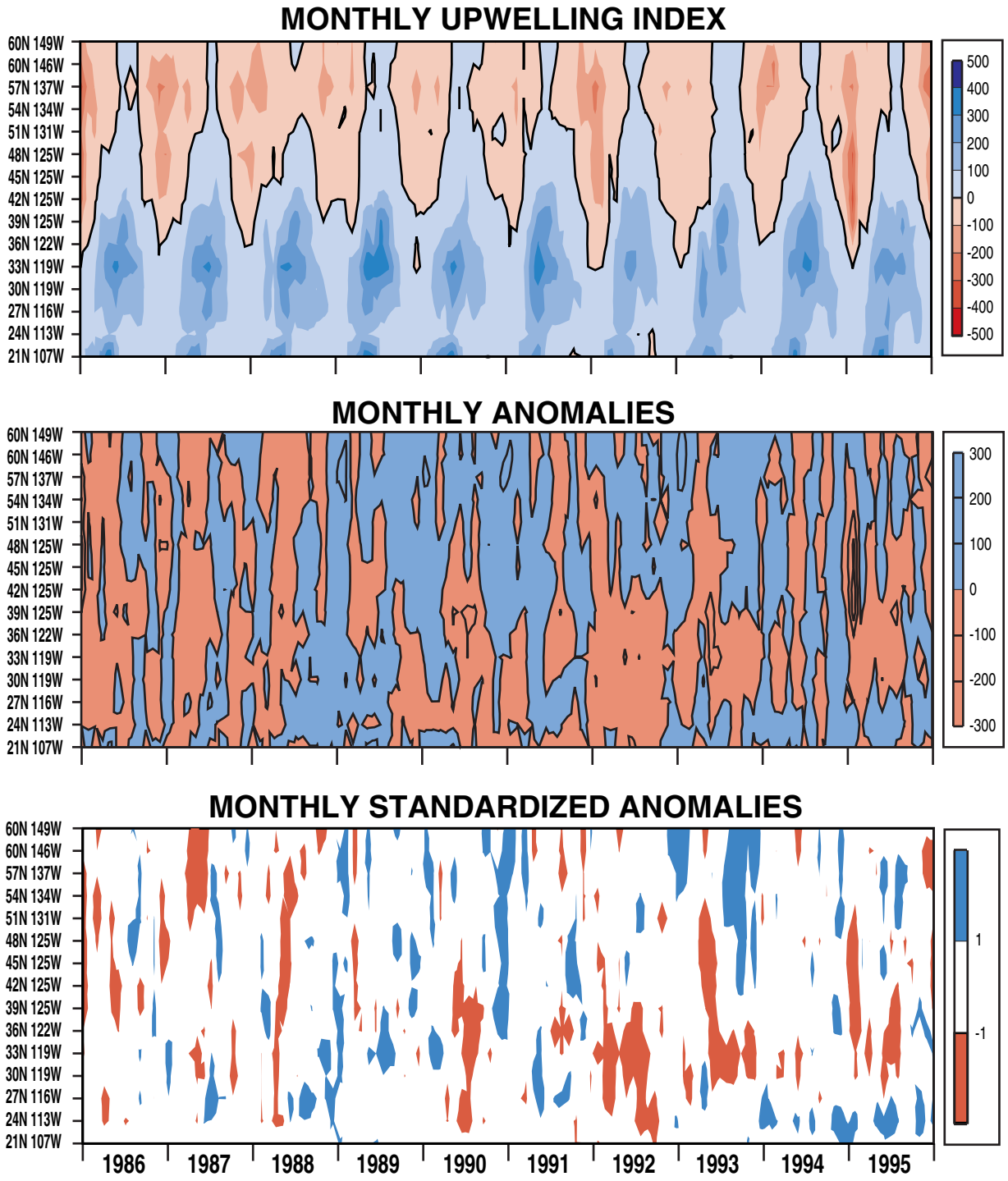
MONTHLY UPWELLING INDEX
60N 149W
60N 146W
57N 137W
54N 134W
51N 131W
48N 125W
45N 125W
42N 125W
39N 125W
36N 122W
33N 119W
30N 119W
27N 116W
24N 113W
21N 107W
500
400
300
200
100
0
-100
-200
-300
-400
-500
MONTHLY ANOMALIES
60N 149W
60N 146W
57N 137W
54N 134W
51N 131W
48N 125W
45N 125W
42N 125W
39N 125W
36N 122W
33N 119W
30N 119W
27N 116W
24N 113W
21N 107W
300
200
100
0
-100
-200
-300
MONTHLY STANDARDIZED ANOMALIES
60N 149W
60N 146W
57N 137W
54N 134W
51N 131W
48N 125W
45N 125W
42N 125W
39N 125W
36N 122W
33N 119W
30N 119W
27N 116W
24N 113W
21N 107W
1
-1
1986
1987
1988
1989
1990
1991
1992
1993
1994
1995